Scientific
Research

Steam Reforming of Ethanol over CoMg/SBA-15 Catalysts

**Josh Y. Z. Chiou[1], Shih-Yi Yang[1], Chin-Liang Lai[1], Hsuan-Ying Kung[1],
Chih-Wei Tang[2], Chen-Bin Wang[1*]**

[1]Department of Chemical and Materials Engineering, Chung Cheng Institute of Technology,
National Defense University, Taoyuan, Chinese Taipei
[2]Department of General Education, Army Academy, Taoyuan, Chinese Taipei
Email: *chenbinwang@gmail.com

ABSTRACT

Hydrogen production through steam reforming of ethanol (SRE) over Mg modified Co-based catalysts supported on mesoporous SBA-15 was studied herein to evaluate the catalytic activity and the behavior of coke deposition. The Co_yMg_x/SBA-15 catalysts are obtained according to the steps of consecutive impregnation of Mg (x = 5 and 10 wt%) to be incorporated on SBA-15 and then follow the loading of Co (y = 10 and 20 wt%) using the incipient wetness impregnation method. The catalysts are characterized by using X-ray diffraction (XRD), temperature programmed reduction (TPR), transmission electron microscopy (TEM) and BET techniques. Also, the spent catalysts are further characterized by using XRD and TEM. The catalytic activity of the SRE is evaluated in a fixed-bed reactor under 22,000 h^{-1} GHSV and with an H_2O/EtOH molar ratio of 13. All the Co_yMg_x/SBA-15 catalysts present a mesoporous structure, even after the SRE reaction. The optimum catalyst of $Co_{20}Mg_5$/SBA-15-H650 comes from the high loading of Co and high reduction temperature pretreatment, which show a high catalytic activity and stability at 550°C with a hydrogen yield (Y_{H2}) up to 5.78 and CO selectivity around 3.10%.

Keywords: SBA-15; Steam Reforming of Ethanol; Cobalt; Magnesium

1. Introduction

Hydrogen generation from biomass-derived alcohols has been the activity of choice recently. Ethanol is more attractive because it is non-toxic, has higher hydrogen content, is renewable energy and has an easy-to-handle nature when compared to methanol [1,2]. The main catalytic reaction using ethanol to produce hydrogen by steam reforming is shown in Equation (1), where only hydrogen and non-renewable CO_2 are produced, providing 6 moles of H_2 per mole of ethanol stoichiometrically [3].

$$C_2H_5OH + 3H_2O \rightarrow 6H_2 + 2CO_2 \qquad (1)$$
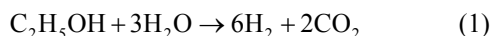
Several metallic active phases have been used as catalysts for the steam reforming of ethanol (SRE) to produce hydrogen. Since Co-based catalysts, mainly metal exhibiting appreciable activity for C-C bond broken and water-gas shift (WGS) reactions, generate a low temperature and few by-products, they are efficient when used in SRE. The early stage of SRE research has focused on Co-based catalysts. Haga *et al.* [4] found that the proper-

ties of cobalt catalysts were greatly influenced by the supports, where the hydrogen production decreased in the order of: $Co/Al_2O_3 > Co/ZrO_2 > Co/MgO > Co/SiO_2 > Co/C$. The Co/Al_2O_3 catalyst showed high hydrogen selectivity for SRE by suppressing CO methanation and ethanol decomposition. Supported cobalt catalysts showed a significant improvement in catalytic performance on the SRE compared with corresponding supports reported by Llorca *et al.* [5], a variety of oxides involving acidic/ basic and redox properties. Batista *et al.* [6] studied the high efficiency SRE over Co/Al_2O_3 and Co/SiO_2 catalysts with little Co content (8%) in which the Co/SiO_2 catalyst showed better CO removal. Llorca *et al.* [7] reported CO-free hydrogen produced from SRE over the Co/ZnO catalyst at low temperatures, where the highly stable catalyst was prepared by using $Co_2(CO)_8$ as a precursor.

The technique of doping extra components, such as alkali (Li, Na and K) [8], alkaline earth (Mg and Ca) [9, 10] and lanthanide (La and Ce) [10] to modify the original property and improve the performance of a catalyst is interesting. Pigos *et al.* [8] reported that the addition of Na and K significantly improved the formate decomposi-

---

tion rate on a WGS reaction over Pt/ZrO₂ catalysts. Wang *et al.* [9] reported that the addition of Na improved the catalytic performance of a PtRu/ZrO₂ catalyst on the oxidative steam reforming of ethanol, where the Na not only enhanced the WGS reaction at a low temperature, but also reduced coke deposition. Cheng *et al.* [10] also reported the promotional effect of doping alkaline earth oxides or lanthanide oxides on a Ni/Al₂O₃ catalyst for CO_2 reforming of CH_4.

Besides the selection of an active metal or promoter for the supported catalysts, the choice of a support with a high surface area to disperse the metal phase over their surface is a main consideration to enhance catalytic performance. Support material, such as γ-Al₂O₃, SiO₂, ZSM-5 [11], MCM-41 [12] and SBA-15 [13], have been widely used in recent years as catalyst supports for catalytic re-actions occurring at high temperatures, based on the support material's larger pores, thicker walls and higher thermal stability. Of considerable interest in this regard are mesoporous materials as a support that will provide an improvement on hydrogen production via steam re-forming reaction [14-19]. The promoter effect of alkaline earth metals (Mg and Ca) over Cu-Ni/SBA-15 [16] and Cu-Ni/SiO₂ [18] catalysts has been studied; both of them improved the dispersion of the metallic phase and strengthened the metal-support interaction. High hydro-gen selectivity was obtained with Mg and reduced depos-ited carbon with the incorporation of Ca. A promoter made up of a $Ce_xZr_{1-x}O_2$ layer pre-coated on SBA-15 changes the redox properties and enhances the catalytic activity on steam reforming of methane over a Ni-based catalyst, as reported by Wang *et al.* [19].

It is well known that Co-based catalysts suffer from deactivation by carbon deposition at high reaction tem-peratures [20]. This is obviously an important point to consider in SRE reactions related to Co-based catalysts. The SBA-15 supported Co catalysts with high surface area and modified by an Mg promoter were prepared in this work. The catalytic performance and coking behav-ior of hydrogen production via SRE over mesoporous structure catalysts were also considered.

2. Experimental

2.1. Catalyst Preparation

SBA-15 was prepared according to the method described in the literature [13]. Briefly, a triblock copolymer P123 (8 g, Strem) was dissolved in 250 mL HCl (1.9 M). The solution was stirred at 40˚C for 2 h, and 16 g of tetraethyl orthosilicate (TEOS) were then slowly added to the mix-ture and stirred vigorously at 40˚C for 22 h. The solution was transferred into a Teflon bottle and aged at 100˚C for 24 h. The solid product was filtered, washed with de-ionized water and then dried at room temperature for 24

h, followed by calcination in air at 500˚C for 6 h with a heating rate of 7˚C /min.

Catalysts promoted with alkaline are much more sen-sitive to the preparation order for catalytic performance, and the promoting effect is more significant when the support is impregnated with the promoter oxides before the incorporation of the active phase [10]. For this reason, Mg-modified Co/SBA-15 catalysts are prepared by con-secutive impregnation with Mg and then Co. Mg$_x$/SBA-15 samples were prepared from the aqueous solution of Mg(NO₃)₂·6H₂O (Mg loading, x = 5 and 10 wt%, Showa) incorporating SBA-15 by the impregnation method. Co$_y$Mg$_x$/SBA-15 samples were prepared by the incipient wetness impregnation method using Mg$_x$/SBA-15 with aqueous Co(NO₃)₂·6H₂O (Co loading, y = 10 and 20 wt%, Showa). All samples were dried at 100˚C overnight and then calcined at 300˚C for 3 h.

2.2. Catalyst Characterization

The metal loading of catalysts was determined by the atomic-emission technique (ICP-AES) using a Perkin Elmer Optima 3000 DV. The BET surface area and pore size distribution were measured by N₂ adsorption at a liquid nitrogen temperature using a Micromeritics ASAP 2010 analyzer. X-ray diffraction (XRD) measurement was performed using a Siemens D5000 diffractometer with Cu K$_{\alpha 1}$ radiation (λ = 1.5406 Å) at 40 kV and 30 mA. The microstructure and particle size of the samples were ob-served by using transmission electron microscopy (TEM) with a JEOL JEM-2010 microscope equipped with a field emission electron source and operated at 200 kV. Reduc-tion behavior of Co$_y$Mg$_x$/SBA-15 catalysts was studied by temperature-programmed reduction (TPR). About 50 mg of the sample were heated in a flow of 10% H₂/N₂ gas at a flow rate of 10 ml·min⁻¹. During TPR, the temperature was increased by 7˚C·min⁻¹ from room temperature to 900˚C.

2.3. Activity Tests

Catalytic activity of Co$_y$Mg$_x$/SBA-15 catalysts in an SRE reaction was determined at atmospheric pressure in a fixed-bed flow reactor. 100 mg of the catalyst were placed in a 4 mm i.d. quartz tubular reactor and held by glass-wool plugs. The temperature of the reactor was controlled by heating tape and measured by a thermo-couple (1.2 mm i.d.) at the center of the reactor bed. The feed of the reactants was comprised of a gaseous mixture of ethanol (EtOH), H₂O and Ar (purity 99.9995%, sup-plied by a mass flow controller). The composition of the reactant mixture (H₂O/EtOH/Ar = 37/3/60 vol%) was controlled by the Ar flow stream (22 mL/min) through a saturator (maintained at 120˚C) containing EtOH and H₂O. The gas hourly space velocity (GHSV) was main-

tained at 22,000 h⁻¹ and the H_2O/EtOH molar ratio was 13 (H_2O:EtOH = 80:20 by volume). Prior to reactivity measurement, the catalyst was reduced in 10% H_2 in N_2 for 2 h at 400°C. The SRE activity was tested stepwise, increasing the temperature from 350°C to 550°C. The reaction was carried out online by gas chromatography (GC) with columns of Porapak Q (for CO_2, H_2O, C_2H_4, CH_3CHO, CH_3OCH_3 and EtOH) and using a Molecular Sieve 5 Å (for H_2, CH_4 and CO) for separation. It was also quantitatively analyzed by two sets of thermal conductivity detectors (TCD) on line. Response factors for all products were obtained, and the system was calibrated with appropriate standards before each catalytic test. Activity evaluation of all samples depended on the conversion of ethanol (X_{EtOH}), the distribution of products (mol %) and the yield of hydrogen (Y_{H2}, mol H_2/mol EtOH) according to the following equations.

$$X_{EtOH} = \left(n_{EtOH,\ reacted} / n_{EtOH,\ fed} \right) \times 100\% \qquad (2)$$

$$Y_{H2} = n_{H2-out} / n_{EtOH,\ reacted} \qquad (3)$$

$$S_i = \left(n_i / \sum n_i \right) \times 100\% \qquad (4)$$

where n_i was a mole of products and included H_2.

3. Results and Discussion

3.1. Characterization of Supports and Catalysts

The XRD patterns at small angles of SBA-15, Mg_x/SBA-15 and Co_yMg_x/SBA-15 (x = 5 and 10; y = 10 and 20) samples are shown in **Figure 1**. The SBA-15 support (**Figure 1(a)**) shows a pattern with three well-resolved peaks observed at 2θ values of 0.92°, 1.54° and 1.77° that correspond to the diffraction of (100), (110) and (200) planes, respectively, indicating their ordered 2D hexagonal structure with space group *p6mm* [13]. The *d*-spacing of this structure, calculated from nλ = 2*d*sinθ is 9.6 nm, which is also in the mesoporous range. Both Mg_x/SBA-15 samples (x = 5 and 10) are presented in **Figures 1(b)** and **(c)**, respectively. The intensity of the diffraction peaks of the hexagonal mesostructure decreases gradually with the increase of x from 5 to 10. Moreover, a similar trend can be observed with the decrease in *d*-spacing where the *d*-spacing for x = 5 and 10 are 9.3 and 9.0 nm, respectively. The intensity of diffraction peaks for the Co_yMg_x/SBA-15 (y = 10 and 20) catalysts (**Figures 1(d)-(h)**) decreases with the increase of x and y, and weakens more than the Mg_x/SBA-15 samples. Furthermore, the material composed of a high surface area, larger pores and thicker walls seems to disintegrate with increasing metal loading, raising doubt about the structural integrity.

The N_2 adsorption-desorption analysis of the Co_yMg_x/SBA-15 catalysts is shown in **Figure 2**. All of the samples exhibit a Type IV isotherm with a clear H1-type

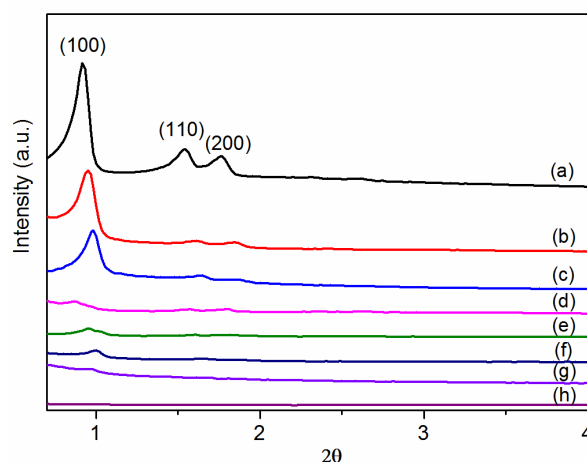**Figure 1. Small angle XRD patterns of the samples: (a) SBA-15 (b) Mg₅/SBA-15 (c) Mg₁₀/SBA-15 (d) Co₁₀Mg₅/SBA-15 (e) Co₂₀Mg₅/SBA-15 (f) Co₂₀Mg₅/SBA-15-H650 (g) Co₁₀Mg₁₀/SBA-15 (h) Co₂₀Mg₁₀/SBA-15.**
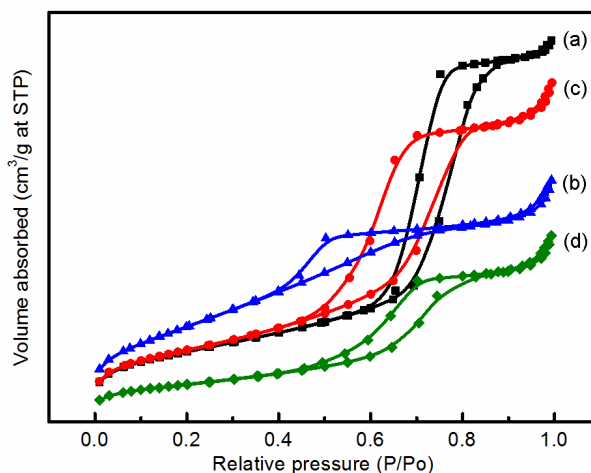
Figure 2. N₂ adsorption/desorption isotherms of the samples: (a) Co₁₀Mg₅/SBA-15 (b) Co₁₀Mg₁₀/SBA-15 (c) Co₂₀Mg₅/SBA-15 (d) Co₂₀Mg₁₀/SBA-15.

hysteresis loop, with metal loading or not (SBA-15 and Mg_x/SBA-15 samples are not shown), which is typical for mesoporous materials. Even though the XRD analysis showed the destruction of the hexagonal structure with impregnation of cobalt, the SBA-15 supported catalysts still maintained the mesoporous structure. **Table 1** summarizes the physical characterization of Co_yMg_x/SBA-15 catalysts, which includes the metal loading, surface area and phase composition. The surface area decreases with the increase of the (x + y) value, where the surface areas are 359, 313, 234 and 130 m^2/g, respectively for the values of 15, 20, 25 and 30. The decrease of surface area indicates that the mesoporous structure may be blocked by large amounts of Mg and Co loading.

The wide-angle XRD patterns of the Co_yMg_x/SBA-15 catalysts are shown in **Figure 3**. The broad and wide

Table 1. Physical characterization of the Co$_y$Mg$_x$/SBA-15 catalysts.

Catalyst	Metal loading (wt %)[a]		Co/Mg ratio (%)	Surface area[b] (m²/g)	Phase[c]
	Co	Mg			
Co$_{10}$Mg$_5$/SBA-15	8.68	4.18	67	359	Co$_3$O$_4$, (Co, Mg)O
Co$_{10}$Mg$_{10}$/SBA-15	9.12	8.24	50	313	Co$_3$O$_4$, (Co, Mg)O
Co$_{20}$Mg$_{10}$/SBA-15	19.0	8.16	67	130	Co$_3$O$_4$, MgCo$_2$O$_4$, (Co, Mg)O
Co$_{20}$Mg$_5$/SBA-15	18.4	4.81	80	234	Co$_3$O$_4$, MgCo$_2$O$_4$, (Co, Mg)O
Co$_{20}$Mg$_5$/SBA-15-H650	18.4	4.81	80	220	MgCo$_2$

[a]ICP-AES measurement. [b]BET measurement. [c]The phase was identified by the XRD and TPR analysis.

peak at 2θ around 15° - 30° is characteristic of amorphous silica. The peak related to MgO ($2\theta \approx 42$°) is unobservable in the XRD patterns for Co$_y$Mg$_x$/SBA-15 catalysts, which indicate the Mg shows highly dispersed on SBA-15 or becomes the nickel-magnesia solution oxides (Co, Mg)O [21,22]. Both the Co10Mg5/SBA-15 and Co10Mg10/SBA-15 catalysts (**Figure 3(a)** and (**b**)) show the characteristic diffraction peaks corresponding to the (220), (311), (511) and (440) planes at 31.3°, 36.8°, 59.0° and 64.8°, respectively. These are related to the cubic phase of Co$_3$O$_4$ (JCPDS No: 76-1802). The spinel structure of magnesium cobaltite MgCo$_2$O$_4$ [23,24] (JCPDS No: 81-0671) shows the corresponding planes of (111), (220), (311), (400), (511) and (440) at 18.9°, 31.1°, 36.6°, 44.5°, 58.9° and 64.7°, respectively. These are obtained on the high Co loading catalysts of Co20Mg5/SBA-15 and Co20Mg10/SBA-15 (**Figures 3(c)** and (**d**)). Otherwise, the higher Co loading would show the stronger diffraction signal. In here, both the Co$_3$O$_4$ and MgCo$_2$O$_4$ phases are not able to give clear assignment, because their diffraction peaks are overlapped. Choudhary *et al*. [25] reported that the MgCo$_2$O$_4$ phase was only observed in the case of catalysts with high Co loadings, such as over 20%, which was supported by our results when y = 20. Therefore, the Co$_y$Mg$_x$/SBA-15 catalysts may contain two phases of Co$_3$O$_4$ and MgCo$_2$O$_4$, and further investigation will be discussed on TPR analysis.

Figure 4 shows the TPR profiles of the Co$_y$Mg$_x$/SBA-15 catalysts. There are two continuous reduction peaks around 180°C to 350°C and broad peak around 500°C to 700°C, respectively. While the lower temperature peaks may be related to the two-steps reduction of Co$_3$O$_4$ [26] and the higher temperature peak is assigned the reduction of MgCo$_2$O$_4$ [25]. Besides, a faint peak over 800°C may be attributed to the reduction of cobalt-magnesia solid solution oxides (Co, Mg)O formed on the catalysts [27]. Further, the reduction signal of Co$_3$O$_4$ would be raised by increasing the Co loading. These results are confirmed to the XRD study, the Co$_3$O$_4$ and MgCo$_2$O$_4$ phases are co-existing in Co$_y$Mg$_x$/SBA-15 catalysts. Particularly, the
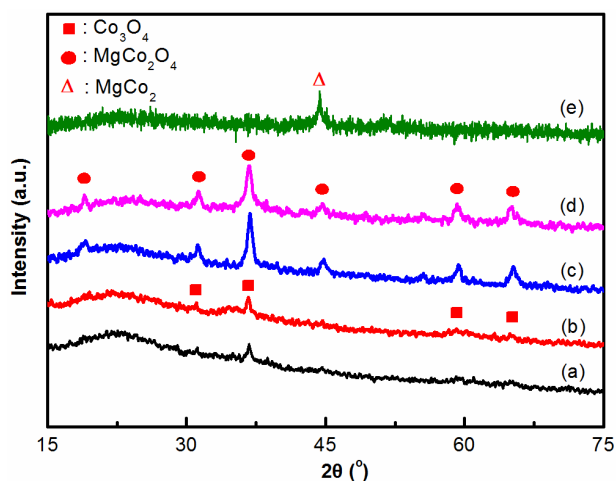
Figure 3. Wide angle XRD patterns of the samples: (a) Co$_{10}$Mg$_5$/SBA-15 (b) Co$_{10}$Mg$_{10}$/SBA-15 (c) Co$_{20}$Mg$_5$/SBA-15 (d) Co$_{20}$Mg$_{10}$/SBA-15 (e) Co$_{20}$Mg$_5$/SBA-15-H650.
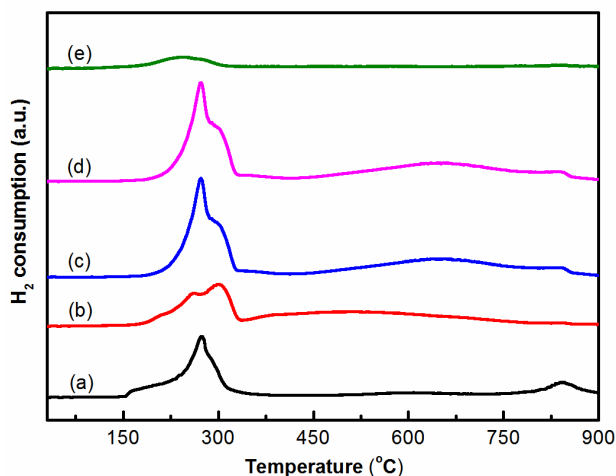
Figure 4. TPR profiles of the samples: (a) Co$_{10}$Mg$_5$/SBA-15 (b) Co$_{10}$Mg$_{10}$/SBA-15 (c) Co$_{20}$Mg$_5$/SBA-15 (d) Co$_{20}$Mg$_{10}$/SBA-15 (e) Co$_{20}$Mg$_5$/SBA-15-H650.

lower Mg loading will product the less amount of MgCo$_2$O$_4$ phase.

3.2. Catalytic Performance

Catalytic performance of ethanol conversion (X_{EtOH}), products distribution and hydrogen yield (Y_{H2}) for the $Co_yMg_x/SBA-15$ catalysts are summarized in **Table 2**. The X_{EtOH} reaches completion for $Co_{10}Mg_5/SBA-15$, $Co_{10}Mg_{10}/SBA-15$ and $Co_{20}Mg_{10}/SBA-15$ catalysts as the reaction temperature (T_R) approaches 475°C; while the Y_{H2} only approaches less than 2.0 at 550°C. Otherwise, both the $Co_{20}Mg_5/SBA-15$ $Co_{20}Mg_5/SBA-15-H650$ catalysts show that the Y_{H2} increases with T_R and up to 5.02 and 5.78, respectively at 550°C.

Table 2. Products distribution of SRE reaction over $Co_yMg_x/SBA-15$ catalysts.

| Catalyst	T_R (°C)	X_{EtOH} (%)	Products distribution (%)[a]						Y_{H2}
			H_2	CH_4	CO	CO_2	C_2H_4	C_2H_4O	
$Co_{10}Mg_5/SBA-15$	400	44.4	44.2	0	0	0	16.7	38.4	0.73
	425	52.6	44.9	0.14	0	0	17.2	38.6	0.76
	450	90.0	45.6	0.42	0.03	0	17.5	38.5	0.79
	475	100	46.1	0.79	0.64	0	17.5	40.7	0.87
	500	100	46.4	1.75	1.15	1.24	9.29	40.2	0.90
	525	100	54.2	8.73	4.73	4.72	7.41	20.2	1.48
	550	100	52.6	11.3	6.38	4.68	6.07	18.9	1.46
$Co_{10}Mg_{10}/SBA-15$	400	57.3	39.6	0.08	0	0	19.7	40.6	0.66
	425	76.2	40.6	0.22	0	0	20.2	39.1	0.68
	450	97.4	41.6	0.51	0.11	0	20.3	37.5	0.72
	475	100	44.5	1.23	0.62	1.56	18.6	33.6	0.83
	500	100	48.1	3.28	2.02	3.24	14.5	28.9	1.01
	525	100	50.4	6.81	3.54	4.75	11.2	23.3	1.20
	550	100	51.4	13.2	6.38	7.13	8.39	13.5	1.46
$Co_{20}Mg_{10}/SBA-15$	400	41.5	44.6	0	0	0	11.7	43.7	1.18
	425	72.6	41.9	0.15	0	0	17.4	40.5	1.18
	450	83.8	41.5	0.29	0	0.44	20.0	37.8	1.33
	475	100	46.9	0.64	0.26	1.22	24.5	26.5	1.48
	500	100	49.2	1.76	1.40	2.12	22.1	23.5	1.73
	525	100	49.7	2.05	1.84	2.21	21.3	23.0	1.70
	550	100	59.2	6.12	4.92	4.14	12.5	13.2	1.86
$Co_{20}Mg_5/SBA-15$	400	31.1	35.5	0.39	0	0	13.3	50.8	0.55
	425	51.5	40.7	0.44	1.46	0	12.4	45.1	0.70
	450	100	47.0	1.81	6.16	0	12.5	32.5	0.96
	475	100	60.3	5.43	11.1	8.54	9.41	5.15	2.22
	500	100	70.0	4.21	8.00	16.7	1.17	0	4.48
	525	100	71.4	4.49	3.54	20.6	0	0	4.99
	550	100	71.5	4.07	3.88	20.5	0	0	5.02
$Co_{20}Mg_5/SBA-15-H650$	400	32.9	52.0	0.06	0.47	5.37	0	42.1	1.15
	425	100	62.7	6.68	16.9	2.25	0	11.5	2.97
	450	100	74.4	6.98	1.48	17.2	0	0	5.56
	475	100	74.4	4.79	1.80	19.0	0	0	5.60
	500	100	74.2	3.43	2.38	19.8	0	0	5.76
	525	100	74.3	3.20	3.05	19.5	0	0	5.78
	550	100	74.3	3.15	3.10	19.6	0	0	5.78

[a]Water is not included.

Based on the phase diagram of the Mg-Co system [28], there is an equilibrium phase for $MgCo_2$ when Co loading is over 67%. Two conditions are required to obtain $MgCo_2O_4$: a high Co loading over 20 wt% [25] and a Co/Mg ratio over 67% [28]. In regard to the pretreatment with reduction temperature effects for the sample with a Co/Mg ratio over 67%, a εCo structure is the major type for a reduction temperature below 422˚C. Otherwise, an αCo structure shows for a reduction temperature over 422˚C [28]. Compared to the pretreatment of temperature effects, a $Co_{20}Mg_5$/SBA-15 catalyst is reduced by H_2 at 650˚C for 2 h (denoted as $Co_{20}Mg_5$/SBA-15-H650). The XRD characterization is shown in **Figure 3(e)** and the TPR analysis is shown in **Figure 4(e)**. The XRD of $Co_{20}Mg_5$/SBA-15-H650 catalyst presences only a diffraction peak around 45˚C that can be identified and assigned to the (400) plane of the $MgCo_2$ phase (JCPDS No. 29-0486). Since the $Co_{20}Mg_5$/SBA-15-H650 sample is storage in atmosphere, the oxidation of sample may be occurred. A TPR profile of $Co_{20}Mg_5$/SBA-15-H650 shows a weak peak below 350˚C which relates to the reduction of Co_3O_4.

In order to understand the variation in the Co/Mg ratio over 67% and pretreatment with the reduction temperature effect, both the $Co_{20}Mg_5$/SBA-15 and $Co_{20}Mg_5$/SBA-15-H650 samples are further discussed. Temperature profiles of catalytic performance on the SRE reaction over the $Co_{20}Mg_5$/SBA-15 and $Co_{20}Mg_5$/SBA-15-H650 samples are described in **Figures 5** and **6**. There are significant differences in catalytic activity and products distribution due to the high temperature reduction. The $Co_{20}Mg_5$/SBA-15-H650 sample is better than the $Co_{20}Mg_5$/SBA-15 sample. The results indicate that the X_{EtOH} approaches completion around 425˚C for $Co_{20}Mg_5$/SBA-15-H650 samples while requiring 450˚C for $Co_{20}Mg_5$/SBA-15 samples to complete the conversion. The Y_{H2} increases up to 5.78 and S_{CO} is 3.10% for the $Co_{20}Mg_5$/SBA-15-H650 sample, while the Y_{H2} approaches 5.02 and S_{CO} is 3.88% for the $Co_{20}Mg_5$/SBA-15 sample at 550˚C. Dehydration especially from ethanol to ethylene is a dominant reaction for all samples that are not pretreated under high temperature reduction, where the selectivity of C_2H_4 is over 10%.

$$C_2H_5OH \rightarrow C_2H_4 + H_2O \qquad (5)$$

The main reaction is the dehydrogenation of ethanol to acetaldehyde at low temperature. As the temperature raised, a major reaction proceeded the decomposition of acetaldehyde into methane and CO for $Co_{20}Mg_5$/SBA-15 and $Co_{20}Mg_5$/SBA-15-H650 samples.

$$C_2H_5OH \rightarrow CH_3CHO + H_2 \qquad (6)$$

$$CH_3CHO \rightarrow CH_4 + CO \qquad (7)$$
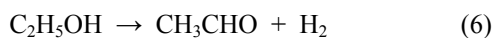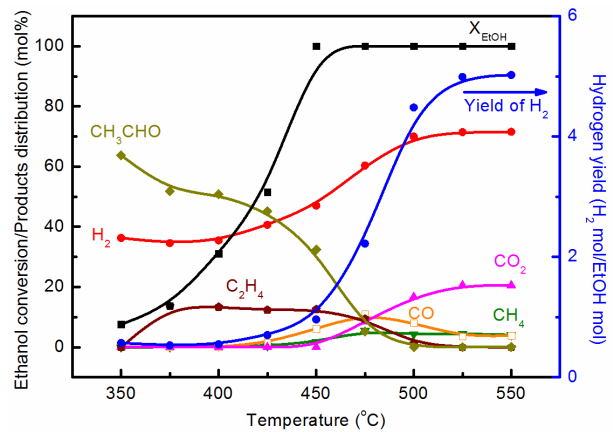
Comparing the temperature effect on the decomposi-

Figure 5. Catalytic performance of SRE reaction over $Co_{20}Mg_5$/SBA-15 catalyst.

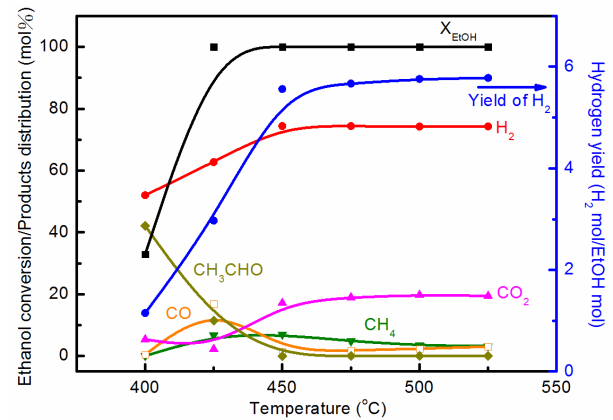**Figure 6. Catalytic performance of SRE reaction over $Co_{20}Mg_5$/SBA-15-H650 catalyst.**

tion of acetaldehyde (D_T), shows that the easy cracking of acetaldehyde promotes the increase of hydrogen yield. However, the promoting effect of a $Co_{20}Mg_5$/SBA-15-H650 sample is more pronounced than that of a $Co_{20}Mg_5$/SBA-15 sample. The D_T of a $Co_{20}Mg_5$/SBA-15-H650 sample is lower than 400˚C, while it is above 450˚C for a $Co_{20}Mg_5$/SBA-15 sample.

The distribution of CO is minor when the T_R is above 425˚C for a $Co_{20}Mg_5$/SBA-15-H650 sample. This demonstates that the water-gas shift reaction (WGSR) is an important side-reaction in the SRE reaction producing H_2 and CO_2.

$$CO + H_2O \rightarrow CO_2 + H_2 \qquad (8)$$
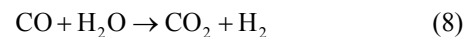
At 525˚C, the selectivity of CH_4, CO and CO_2 arrive at 3.20%, 3.05% and 19.5%, respectively, for a $Co_{20}Mg_5$/SBA-15-H650 sample. The hydrogen selectivity is close to its stoichiometric value (75%), whereas an increase of up to 74% is obtained at over 450˚C. Unlike the $Co_{20}Mg_5$/SBA-15 and $Co_{20}Mg_5$/SBA-15-H650 samples, other Co_yMg_x/SBA-15 catalysts show poor catalytic performance in an SRE reaction. The low H_2 yields (<1.9)

and CO_2 selectivity are produced by the ethanol dehydration to ethylene followed by steam reforming, where C_2H_4 is up to 20% at 450˚C. However, the formation of carbon through C_2H_4 is a possible route, which leads to catalyst deactivation.

$$C_2H_4 \rightarrow polymer \rightarrow coke \qquad (9)$$
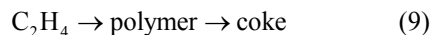
3.3. Characterization of Used Catalyst

XRD and TEM analysis are used to characterize the Co_yMg_x/SBA-15 catalysts after the SRE reaction. XRD patterns reveal MgO (JCDPS No. 4-829) and CoO (JCDPS No. 78-0431) diffraction patterns on $Co_{10}Mg_5$/SBA-15, $Co_{10}Mg_{10}$/SBA-15 and $Co_{20}Mg_{10}$/SBA-15 samples (**Figures 7(a), (b)** and **(e)**). Only the $Co_{20}Mg_5$/SBA-15 and $Co_{20}Mg_5$/SBA-15-H650 samples show metallic Co (JCDPS No. 89-4307) reflections of (111) and (200) planes (**Figures 7(c)** and **(d)**). These results are in good agreement, helping to convince researchers that the $Co_{20}Mg_5$/SBA-15 and $Co_{20}Mg_5$/SBA-15-H650 samples show the better catalytic activity than others in an SRE reaction, exhibiting an active site of metallic Co. The metallic Co usually generated via the reduction of Co_3O_4, which was easily sintered if the interaction with the support was absent [27]. However, the $Co_{20}Mg_5$/SBA-15 and $Co_{20}Mg_5$/SBA-15-H650 samples could form $MgCo_2O_4$ or $MgCo_2$ phases and formatted well-dispersed Co clusters, which are more resistant to sintering due to a stronger interaction between MgO and the support [25]. Based on previous reports [27,29], coke formation would not be stimulated on well-dispersed Co clusters to deactivate the catalyst.

The TEM images (**Figure 8**) show that carbon deposited as large filaments and tubes emerged with the catalyst particles and/or as an amorphous coating carbon on
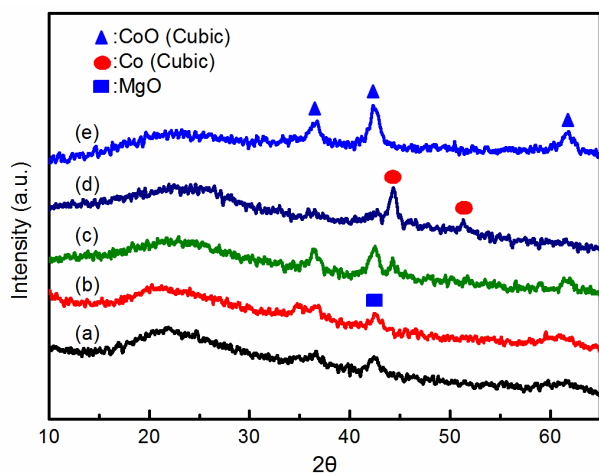

Figure 8. TEM images of spent catalysts: (a) $Co_{10}Mg_5$/SBA-15 (b) $Co_{10}Mg_{10}$/SBA-15 (c) $Co_{20}Mg_5$/SBA-15 (d) $Co_{20}Mg_5$/SBA-15-H650 (e) $Co_{20}Mg_{10}$/SBA-15.

the catalyst particles. The filaments and tubes carbon is shown in the $Co_{20}Mg_5$/SBA-15 and $Co_{20}Mg_5$/SBA-15-H650 samples (**Figures 8(c)** and **(d)**), and amorphous carbon is presented in the $Co_{10}Mg_5$/SBA-15, $Co_{10}Mg_{10}$/SBA-15 and $Co_{20}Mg_{10}$/SBA-15 catalysts (**Figures 8(a)**, **(b)** and **(e)**). According to the deactivation with the deposited carbon, the coating carbon could shorten the lifetime of a catalyst rather than filaments carbon [30], which agreed with our results. Moreover, all the samples maintain a mesoporous structure of SBA-15 after the SRE reaction. A good thermal stability is presented.

4. Conclusion

Steam reforming of ethanol was studied over SBA-15 supported catalysts with a Mg promoter and a cobalt loading of 10 and 20 wt%. The Co/Mg ratio and pretreatment of catalysts play a major role on the catalytic performance regarding the structural properties. A high catalytic performance and hydrogen yield were obtained on the high loading of Co, where the Co/Mg ratio was 0.8. According to the phase diagram of an Mg-Co system,

Figure 7. Wide angle XRD patterns of spent catalysts: (a) $Co_{10}Mg_5$/SBA-15 (b) $Co_{10}Mg_{10}$/SBA-15 (c) $Co_{20}Mg_5$/SBA-15 (d) $Co_{20}Mg_5$/SBA-15-H650 (e) $Co_{20}Mg_{10}$/SBA-15.

a reduction temperature of 650˚C would form $MgCo_2$ as the main phase convinced by XRD, which leads to the active site to enhance the catalytic performance. The Y_{H2} approaches 5.78 and the S_{CO} is 3.10% for $Co_{20}Mg_5$/SBA-15-H650 sample as the T_R approaches 550˚C.

5. Acknowledgements

REFERENCES

[1] R. D. Cortright, R. R. Davda and J. A. Dumesic, "Hydrogen from Catalytic Reforming of Biomass-Derived Hydrocarbons in Liquid Water," *Nature*, Vol. 418, No. 6901, 2002, pp. 964-967. doi:10.1038/nature01009

[2] D. K. Liguras, D. I. Kondarides and X. E. Verykios, "Production of Hydrogen For Fuel Cells by Steam Reforming of Ethanol over Supported Noble Metal Catalysts," *Applied Catalysis B*: *Environmental*, Vol. 43, No. 4, 2003, pp. 345-354. doi:10.1016/S0926-3373(02)00327-2

[3] P. Ramirez de la Piscina and N. Homs, "Use of Biofuels to Produce Hydrogen (Reformation Processes)," *Chemical Society Review*, Vol. 37, No. 11, 2008, pp. 2459-2467. doi:10.1039/b712181b

[4] F. Haga, T. Nakajima, H. Miya and S. Mishima, "Catalytic Properties of Supported Cobalt Catalysts for Steam Reforming of Ethanol," *Catalysis Letters*, Vol. 48, No. 3-4, 1997, pp. 223-227. doi:10.1023/A:1019039407126

[5] J. Llorca, N. Homs, J. Sales and P. Ramirez de la Piscina, "Efficient Production of Hydrogen over Supported Cobalt Catalysts from Ethanol Steam Reforming," *Journal of Catalysis*, Vol. 209, No. 2, 2002, pp. 306-317. doi:10.1006/jcat.2002.3643

[6] M. C. Batista, R. K. S. Santos, E. M. Assaf, J. M. Assaf and E. A. Ticianelli, "High Efficiency Steam Reforming of Ethanol by Cobalt-Based Catalysts," *Journal of Power Sources*, Vol. 134, No. 1, 2004, pp. 27-32. doi:10.1016/j.jpowsour.2004.01.052

[7] J. Llorca, P. Ramirez de la Piscina, J.-A. Dalmon, J. Sales and N. Homs, "CO-Free Hydrogen from Steam-Reforming of Bioethanol over ZnO-Supported Cobalt Catalysts Effect of the Metallic Precursor," *Applied Catalysis B*: *Environmental*, Vol. 43, No. 4, 2003, pp. 355-369. doi:10.1016/S0926-3373(02)00326-0

[8] J. M. Pigos, C. J. Brooks, G. Jacobs and B. H. Davis, "Low Temperature Water-gas Shift: The Effect of Alkali Doping on the C-H Bond of Formate over Pt/ZrO_2 Catalysts," *Applied Catalysis A*: *General*, Vol. 328, No. 1, 2007, pp. 14-26. doi:10.1016/j.apcata.2007.04.001

[9] C. H. Wang, K. F. Ho, J. Y. Z. Chiou, C. L. Lee, S. Y. Yang, C. T. Yeh and C. B. Wang, "Oxidative Steam Reforming of Ethanol over PtRu/ZrO_2 Catalysts Modified with Sodium and Magnesium," *Catalysis Communica-*

tions, Vol. 12, No. 10, 2011, pp. 854-858. doi:10.1016/j.catcom.2011.02.002

[10] Z. Cheng, Q. Wu, J. Li and Q. Zhu, "Effects of Promoters and Preparation Procedures on Reforming of Methane with Carbon Dioxide over Ni/Al_2O_3 Catalyst," *Catalysis Today*, Vol. 30, No. 1-3, 1996, pp. 147-155. doi:10.1016/0920-5861(95)00005-4

[11] D. H. Olson, G. T. Kokotailo, S. L. Lawton and W. M. Meler, "Crystal Structure and Structure-Related Properties of ZSM-5," *The Journal of Physical Chemistry*, Vol. 85, No. 15, 1981, pp. 2238-2243. doi:10.1021/j150615a020

[12] C. T. Kresge, M. E. Leonowicz, W. J. Roth, J. C. Vartuli and J. S. Beck, "Ordered Mesoporous Molecular Sieves Synthesized by a Liquid-crystal Template Mechanism," *Nature*, Vol. 359, No. 6397, 1992, pp. 710-712. doi:10.1038/359710a0

[13] D. Zhao, J. Feng, Q. Huo, N. Melosh, G. H. Fredrickson, B. F. Chmelka and G. D. Stucky, "Triblock Copolymer Syntheses of Mesoporous Silica with Periodic 50 to 300 Angstrom Pores," *Science*, Vol. 279, No. 5350, 1998, pp. 548-552. doi:10.1126/science.279.5350.548

[14] A. J. Vizcaíno, A. Carrero and J. A. Calles, "Hydrogen Production by Ethanol Steam Reforming over Cu-Ni Supported Catalysts" *International Journal of Hydrogen Energy*, Vol. 32, No. 10-11, 2007, pp. 1450-1461. doi:10.1016/j.ijhydene.2006.10.024

[15] A. Carrero, J. A. Calles and A. J. Vizcaíno, "Hydrogen Production by Ethanol Steam Reforming over Cu-Ni/ SBA-15 Supported Catalysts Prepared by Direct Synthesis and Impregnation," *Applied Catalysis A*: *General*, Vol. 327, No. 1, 2007, pp. 82-94. doi:10.1016/j.apcata.2007.04.030

[16] A. J. Vizcaíno, A. Carrero and J. A. Calles, "Ethanol Steam Reforming on Mg- and Ca-modified Cu-Ni/SBA-15 Catalysts," *Catalysis Today*, Vol. 146, No. 1-2, 2009, pp. 63-70. doi:10.1016/j.cattod.2008.11.020

[17] J. A. Calles, A. Carrero and A. J. Vizcaíno, "Ce and La Modification of Mesoporous Cu-Ni/SBA-15 Catalysts for Hydrogen Production through Ethanol Steam Reforming," *Microporous and Mesoporous Materials*, Vol. 119, No. 1-3, 2009, pp. 200-207. doi:10.1016/j.micromeso.2008.10.028

[18] A. Carrero, J. A. Calles and A. J. Vizcaino, "Effect of Mg and Ca Addition on Coke Deposition over Cu-Ni/SiO_2 Catalysts for Ethanol Steam Reforming," *Chemical Engineering Journal*, Vol. 163, No. 3, 2010, pp. 395-402. doi:10.1016/j.cej.2010.07.029

[19] K. Wang, X. Li, S. Ji, X. Shi and J. Tang, "Effect of $Ce_xZr_{1−x}O_2$ Promoter on Ni-Based SBA-15 Catalyst for Steam Reforming of Methane," *Energy & Fuels*, Vol. 23, No. 1, 2009, pp. 25-31. doi:10.1021/ef800553b

[20] H. Wang, Y. Liu, L. Wang and Y. Qin, "Study on the Carbon Deposition in Steam Reforming of Ethanol over Co/CeO_2 Catalyst," *Chemical Engineering Journal*, Vol. 145, No. 1, 2008, pp. 25-31. doi:10.1016/j.cej.2008.02.021

[21] B. Huang, X. Li, S. Ji, B. Lang, F. Habimana and C. Li, "Effect of MgO Promoter on Ni-based SBA-15 Catalysts

for Combined Steam and Carbon Dioxide Reforming of Methane," *Journal of Natural Gas Chemistry*, Vol. 17, No. 3, 2008, pp. 225-231.
doi:10.1016/S1003-9953(08)60055-9

[22] W. Liu, S. Y. Lai, H. X. Dai, S. J. Wang, H. Z. Sun and C. T. Au, "MgO-Modified VO_x/SBA-15 as Catalysts for the Oxidative Dehydrogenation of *n*-Butane," *Catalysis Today*, Vol. 131, No. 1-4, 2008, pp. 450-456.
doi:10.1016/j.cattod.2007.10.054

[23] M. A. Zamudio, S. Bensaid, D. Fino and N. Russo, "Influence of the $MgCo_2O_4$ Preparation Method on N_2O Catalytic Decompositio," *Industrial & Engineering Chemistry Research*, Vol. 50, No. 5, 2011, pp. 2622-2627.
doi:10.1021/ie100658w

[24] Y. Sharma, N. Sharma, G. V. Subba Rao and B. V. R. Chowdari, "Studies on Spinel Cobaltites, $FeCo_2O_4$ and $MgCo_2O_4$ as Anodes for Li-ion batteries," *Solid State Ionics*, Vol. 179, No. 15-16, 2008, pp. 587-597.
doi:10.1016/j.ssi.2008.04.007

[25] V. R. Choudhary, K. C. Mondal and T. V. Choudhary, "CO_2 Reforming of Methane to Syngas over CoO_x/MgO Supported on Low Surface Area Macroporous Catalyst Carrier: Influence of Co Loading and Process Conditions," *Industrial & Engineering Chemistry Research*, Vol. 45, No. 13, 2006, pp. 4597-4602.
doi:10.1021/ie060260a

[26] C. B. Wang, C. C. Lee, J. L. Bi, J. Siang, J. Y. Liu and C. T. Yeh, "Study on the Steam Reforming of Ethanol over Cobalt Oxides," *Catalysis Today*, Vol. 146, No. 1-2, 2009, pp. 76-81. doi:10.1016/j.cattod.2008.12.010

[27] H. Y. Wang and E. Ruckenstein, "CO_2 Reforming of CH_4 over Co/MgO Solid Solution Catalysts—Effect of Calcination Temperature and Co loading," *Applied Catalysis A*: *General*, Vol. 209, No. 1-2, 2001, pp. 207-215.
doi:10.1016/S0926-860X(00)00753-5

[28] A. A. Nayeb-Hashemi and J. B. Clark, "The Co-Mg (Cobalt-Magnesium) System," *Bulletin of Alloy Phase Diagrams*, Vol. 8, No. 4, 1987, pp. 352-354.

[29] E. Ruckenstein and H. Y. Wang, "Carbon Deposition and Catalytic Deactivation during CO_2 Reforming of CH_4 over Co/γ-Al_2O_3 Catalysts," *Journal of Catalysis*, Vol. 205, No. 2, 2002, pp. 289-293.
doi:10.1006/jcat.2001.3458

[30] I. Suelves, M. J. Lázaro, R. Moliner, B. M. Corbella and J. M. Palacios, "Hydrogen Production by Thermo Catalytic Decomposition of Methane on Ni-Based Catalysts: Influence of Operating Conditions on Catalyst Deactivation and Carbon Characteristics," *International Journal of Hydrogen Energy*, Vol. 30, No. 15, 2005, pp. 1555-1567.
doi:10.1016/j.ijhydene.2004.10.006